Towards Physics Based Strategies for Separation Control over an Airfoil using Synthetic Jets

Reni Raju* and Rajat Mittal†

The George Washington University, Washington, DC 20052

Louis N. Cattafesta III‡

University of Florida, Gainesville, FL 32611

Effect of forcing using a modeled zero-net mass-flux (ZNMF) jet on a stalled NACA 4418 airfoil at R_c=40,000 is examined using two-dimensional numerical simulations. The baseline uncontrolled simulations are modeled after the experiments of Zaman & Culley. The simulations indicate that the stalled airfoil is subject to three naturally occurring frequencies corresponding to the shear layer, the separation bubble, and the wake. The jet forcing frequencies are chosen to match the shear layer and separation bubble frequencies. It is observed that forcing frequencies near the natural separation bubble frequency elicits the best response in terms of separation reduction and increase in lift-to-drag ratios. Using higher forcing frequencies that are close to the shear layer frequency does not reduce separation. However, the shear layer is found to be highly receptive to this forcing leading to a highly organized and coherent rollup and subsequent vortex merging process.

Nomenclature

c	Chord length, m
C_d	Drag coefficient
C_f	Skin friction coefficient
C_l	Lift coefficient
C_μ	Momentum coefficient, $\equiv \rho w_J \int_0^{T/2} V_J(t)^2 dt/(0.5Tcq)$
C_p	Pressure coefficient
F^+	Generic dimensionless forcing frequency
f_J	Jet forcing frequency, Hz
f_{sep}	Frequency of the separation bubble, Hz
f_{SL}	Frequency of the shear layer, Hz
f_{wake}	Frequency of the wake, Hz
H_{sep}	Height of separation bubble, m
L_{sep}	Length of separation bubble, m
q	Dynamic pressure $\equiv 0.5\rho U_\infty^2$
Re_c	Reynolds number based on c
T	Time period of jet
u	Streamwise velocity, m/s
U_∞	Freestream velocity, m/s
v	Cross-stream velocity, m/s
$V_J(t)$	Jet velocity, m/s
V_0	Maximum jet velocity, m/s
w_J	Width of the jet, m

*Graduate Student, Department of Mechanical & Aerospace Engineering, Student member AIAA

†Professor, Department of Mechanical & Aerospace Engineering, Associate Fellow AIAA, mittal@gwu.edu

‡Associate Professor, Department of Mechanical & Aerospace Engineering, Associate Fellow AIAA

x_J Location of the jet center from LE, m

Greek

ρ Density, kg/m^3

α Angle of attack, *degrees*

superscript

$*$ Dimensionless quantity normalized by U_∞/c

I. Introduction

Flow control over aerodynamic surfaces can be effectively achieved through periodic excitation.[1–3] Zero-net mass-flux (ZNMF) devices or "synthetic jets" provide periodic forcing through oscillatory blowing with an essential zero-mean, thus enabling either control/delay of boundary layer separation or global modification of the flow to generate lift while reducing drag.[2,4–7] Studies show that these devices improve aerodynamic performance with significantly less addition of momentum as compared to steady blowing.[2] The fundamental mechanism for the ZNMF actuators is the periodic entrainment and expulsion of outer fluid leading to a periodic addition of momentum or cyclic oscillations to a separating boundary layer thereby improving its ability to overcome an adverse pressure gradient.[8]

Delay and control of stall using ZNMF devices has been studied extensively on several key issues such as optimal forcing frequencies,[2,5,9,10] waveforms,[10,11] momentum coefficient,[2,5,6] location of the actuator[2,6] and curvature effects.[12] The key control parameters of a ZNMF jet are the jet frequency, f_J, and jet velocity, V_J which might be the peak, rms or spatial-averaged velocity during the expulsion phase of a cycle. Although the control authority varies monotonically with V_J/U_∞ up to a point where a further increase completely disrupts the boundary layer, the effectiveness of forcing can be manipulated through V_J/U_∞ by placing the jet upstream of the separation point.[6] On the other hand the control authority has a highly non-monotonic variation with F^+, defined as $F^+ = f_J/f_n$ where f_n is some natural frequency in the uncontrolled flow. In the past, f_n was usually assumed to be associated with the time-scale of the separation region. However, studies have found a large range of F^+ values that provide effective control.[13] This might be indicative of the fact that there is more than one natural time-scale in these flows and that the physical mechanisms underlying ZNMF based separation control are not yet fully understood.

As pointed out by Mittal et al.[13] depending on flow conditions, there are at least three natural frequencies occurring in a separated airfoil flow. Typically at low angles of incidence where the flow remains attached to suction side of airfoil only the global instability causing Karman vortex shedding exists with a dominant frequency, f_{wake}. At higher angles of incidence due to the presence of an adverse pressure gradient separation may occur, usually near the leading edge and the flow might or might not reattach. In case the flow does not reattach then the flow is subject to at least two natural frequencies, f_{wake} and f_{SL}, the latter due to the local shear layer instability. On the other hand if the flow does reattach before the trailing edge a third frequency scale, f_{sep} corresponding to the separation bubble may also be present. The wake frequency scales as $f_{wake} \sim U_{wake}/W_{wake}$,[14] where U_{wake} is flow velocity outside the wake and W_{wake} the width of the wake. On the other hand separation bubble frequency scales as $f_{sep} \sim U_\infty/L_{sep}$, L_{sep} being the length scale of the separation bubble. In such a case where the shear layer separates and reattaches there might be lock-on of f_{SL} to f_{sep} through subharmonic resonance. If, however, the flow does not reattach, this frequency scales like a free shear layer i.e. $\overline{U}/\theta$,[15] where $\overline{U}$ is the average velocity in the shear layer and θ is the momentum thickness. It is plausible to consider the optimal forcing frequency based on these three frequencies such that it provides maximal flow reattachment as measured by mean surface shear stress, $(f_J)_{optimal} = fn(f_{SL}, f_{sep}, f_{wake})$.

The question therefore remains as to which frequency determines the optimal jet frequency. Mittal et al.[13] have reviewed the possibility of a wide range of the optimal values of F^+ based on the various definitions used by researchers. Studies show that for $F^+ = f_J c/U_\infty$, optimal values range from 0.55 to 5.5. For $F^+ = f_J X_{TE}/U_\infty$, X_{TE} being the distance from actuator to trailing edge, this range is found to be 0.5 to 2.0, while for $F^+ = f_J L_{sep}/U_\infty$ optimal values range from 0.75 to 2.0. Overall $F^+ \sim O(1)$ provide better flow control, however in certain cases $F^+ > 10$ have also shown to result in improved aerodynamics performance.[6] Wu et al.[9] have argued that for post-stall cases, the optimal control frequency should be a harmonic of f_{wake}. Due to the ability of the shear layer to respond to a broad range of frequencies a suitable choice for F^+ can allow both the vortex shedding and shear layer to lock-on to the forcing frequency or its

super-harmonic. Hence there is still a need for further investigation of the non-linear interactions of natural instabilities to the forcing frequency.

Mittal et al.,[13] Mittal & Kotapati[16] and Kotapati et al.[17] have presented a novel approach of investigating flow with these three distinct frequency scales in a canonical flow configuration with a separated flow over a thick elliptic plate. It was found that forcing the jet at separation bubble frequency provided the most effective means of suppressing separation with shear layer and separation zone locking on to the forcing frequency or its sub-harmonic. On the other hand, when forcing was provided at frequencies higher than that of the shear layer there was no improvement in separation control. In the present work we examine these issues for a conventional separated airfoil flow. The aim is to examine the detailed flow physics over a stalled airfoil and its response to the forcing frequencies. For this purpose we have chosen a 2-D NACA 4418 airfoil for which experimental drag data is available from Zaman & Culley.[18] They have examined the effects of frequencies and velocity amplitude at a single jet location for post-stall cases at high α. For the present work we have chosen a post-stall case at a moderately high α=18° where the separated flow shows reattachment. It is expected that this flow will contain all three naturally occurring frequencies. Flow control is investigated over a range of frequencies and the effect of two distinct jet locations is also investigated.

II. Flow Configuration

The airfoil configuration chosen for the current study is shown in figure 1. The airfoil is a NACA 4418, based on the experimental setup by Zaman & Culley.[18] The chord Reynolds number is set at Re_c = 40,000 while the domain size is $7c \times 8c$ with the airfoil placed at the origin. Typical grids used range from 386 × 158 to 544 × 168 and figure 2 shows grid topology. Freestream velocity is prescribed at the inflow, while a non-reflecting boundary condition is used at the exit. Slip boundary conditions are prescribed at the top and bottom walls.

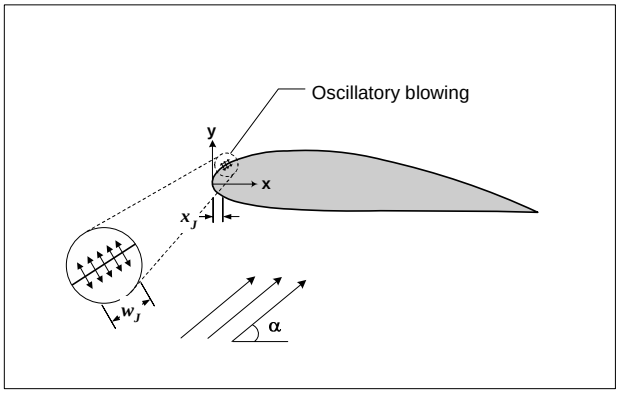

Figure 1. Schematic of the NACA 4418 airfoil used for simulation

For the control cases ZNMF actuator is modeled by providing an oscillatory boundary condition on the airfoil surface at a distance x_J/c from the leading edge of the form $V_0 \sin(\omega t)$. The forcing is provided over the length w_J/c normal to the airfoil surface. All the control simulations are based on baseline flow configuration at α=18°. The summary of the cases are listed in table 1. Each simulation requires about 60-70 hours of CPU time on Intel® Xeon and Compaq GS 320 processors.

III. Numerical Methodology

The simulations employ a sharp interface immersed boundary method (IBM) developed by Ghias et al.[19,20] The method allows for simulation of compressible flow with immersed bodies on non-body conformal grids. The governing equations used are the unsteady, viscous, compressible Navier-Stokes equations written in terms of conservative variables. The equations are transformed to a generalized curvilinear coordinate system, while maintaining the strong conservation form of the equations.[21] The equations are discretized in the computational domain with a cell-centered arrangement using a hybrid second-order central-difference-QUICK scheme,[22] which allows for precise control of the numerical dissipation. The diagonal viscous terms are treated implicitly using a Crank-Nicolson scheme wherein all the other terms including the convective terms and cross-terms are treated explicitly using a low-storage, 3rd - order Runge-Kutta scheme.[23] Using this mixed implicit-explicit scheme virtually eliminates the viscous stability constraint which can be quite severe in simulation of viscous flows. The resulting equations are solved by a LSOR iterative method.[23]

The immersed boundary (IBM) method is used to simulate flow past immersed boundaries on structured curvilinear girds that do not conform to the shape of the boundary and allows us to simulate the airfoil flow on a single-block mesh with no branch cuts. This topology allows us to maintain relatively better grid quality in the entire domain. The geometry of the immersed boundary is defined by a set of marker points connected

by linear segments. Cells whose centers lie inside the immersed body and have at least one neighboring cell with its center located outside the body, are marked as "ghost-cells". The rest of the cells with centers inside the body, which are not adjacent to the immersed boundary, are marked as "solid" cells. The basic idea in this method is to compute the flow variables for the ghost cells such that the boundary conditions on the immersed boundary in the vicinity of the ghost cell are satisfied. Figure 2 shows the curvilinear 2-D grid employed for current study. Use of curvilinear grids allows for the surface of the airfoil to be mostly parallel to the grid lines, maintaining relatively high resolution in the boundary layer. Validation and accuracy tests of this solver against experiments and numerical simulations have been presented elsewhere.[19,20]

Table 1. Jet parameters used for numerical simulation

Case	$f_J c/U_\infty$	x_J/c	w_J/c	V_0/U_∞	C_μ
1	f^*_{sep}	0.024	0.012	0.1	0.00012
2	f^*_{sep}	0.070	0.019	0.1	0.00019
3	$1.5f^*_{sep}$	0.024	0.012	0.1	0.00012
4	$2.0f^*_{sep}$	0.024	0.012	0.1	0.00012
5	$0.8f^*_{SL}$	0.024	0.012	0.1	0.00012
6	f^*_{SL}	0.024	0.012	0.1	0.00012

IV. Results and Discussion

IV.A. Baseline Uncontrolled Case

In order to benchmark the uncontrolled case, the computed drag coefficients have been compared to the experimental results[18] over a range of angles-of-attack. The results shown in figure 3(a) suggest that the 2-D simulations lead to a reasonable prediction of the drag coefficients upto $\alpha = 20°$. For $\alpha > 20°$ the 2-D calculations tend to over-predict the drag which is a clear indication that strong three-dimensional effects are present in the experimental flow.[24] Furthermore, figure 3(b) shows that C_l starts to decrease for $\alpha > 17°$ indicating a stall condition. Results presented henceforth for the baseline and control cases are pertaining to $\alpha = 18°$ which is a post-stall case.

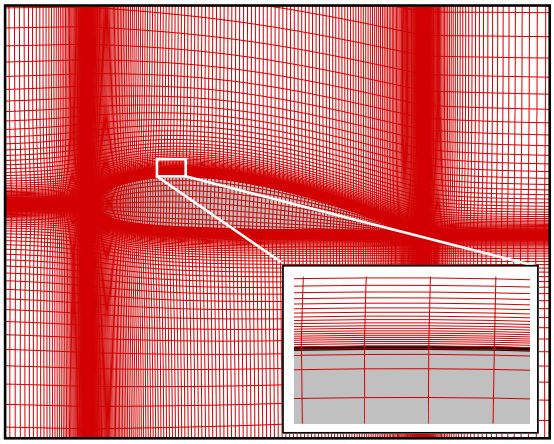

Figure 2. Topology of the grid typically used for the "IBM" simulation, grid size is 384 × 157

Figure 4(a) shows the instantaneous spanwise vorticity plot for the stall case. Separation occurs near the leading edge and the separated shear layer undergoes a Kelvin-Helmholtz instability resulting in vortex rollup. These vortices merge and form larger clockwise vortices which eventually convect downstream. At the trailing edge, the pressure side boundary layer separates and rolls up into counterclockwise vortices which together with the clockwise vortices from the suction side form the "wake" of the airfoil. In order to examine the time-scales associated with the various features of this flow, we have extracted in figure 4(b) the temporal variation of the cross-stream velocity component at the three-locations indicated by white circles in figure 4(a). The streamwise locations of these probes are x/c=0.14, x/c =0.46 and x/c =1.22 which correspond to the shear layer, separated vortices and wake respectively. The corresponding power spectra shown in figure 4(c) indicate that the three distinct naturally occurring frequencies in the flow are f^*_{SL}=10, f^*_{sep}=2 and f^*_{wake}=1. It should be noted that multiple dominant peaks coexist in the spectra and discerning the characteristic frequency is only possible by comparing the corresponding probe data variation over a cycle.

The flow separates near the leading edge of the airfoil at about $x/c = 0.032$ and reattaches at about x/c = 0.76 in the mean as seen from the streamlines of the time-averaged uncontrolled flow shown in figure 5(a). The separation bubble formed due to the adverse pressure gradient has a length, $L_{sep}/c \approx 0.72$ and height,

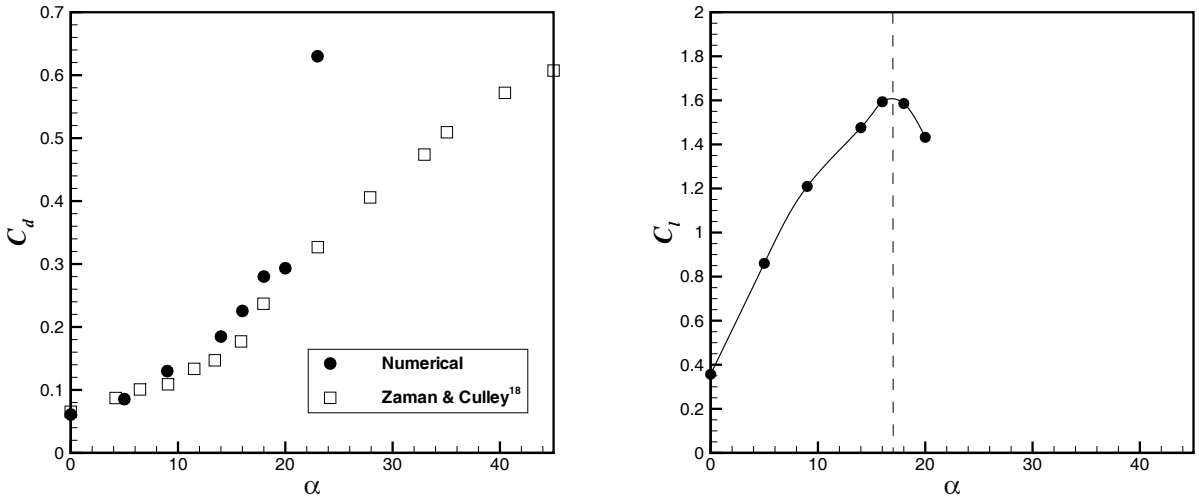

(a) (b)

Figure 3. Variation of (a) the drag coefficient compared with experimental values and (b) the lift coefficient for increasing α.

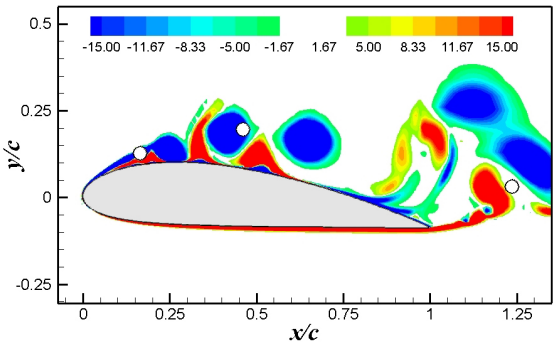

(a)

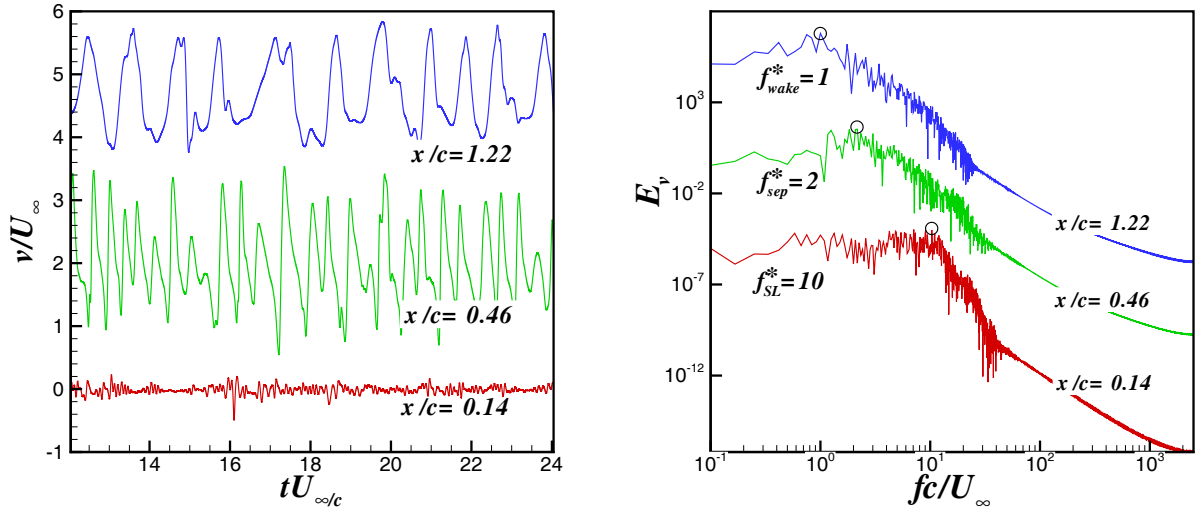

(b) (c)

Figure 4. (a) Instantaneous spanwise vorticity with probe locations; (b) Temporal variation of cross-stream velocity at probe locations x/c =0.14, x/c =0.46 and x/c =1.22, the plots for latter two have been offset by 2 and 4.5 respectively in y-axis for clarity. Corresponding (c) power spectra shows the frequencies for shear layer, separation bubble and wake, offset in y-axis for distinction.

$H_{sep}/c \approx 0.07$. As shown in the inset, a secondary recirculation region extends from $x/c \approx 0.09$ to 0.26. The separation regions can be clearly identified from the corresponding skin friction on the airfoil surface shown in figure 5(b). The plot also shows that the separation affects the pressure recovery near the leading edge of the airfoil.

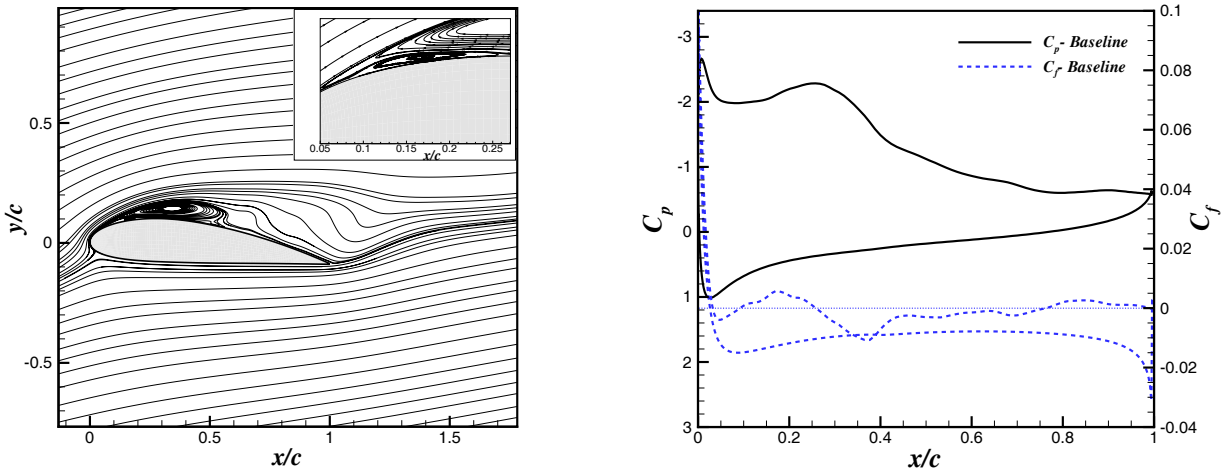

(a) (b)

Figure 5. Plots of time-averaged (a) streamlines, (b) C_p and C_f over the airfoil surface (the dotted line represents zero mean for C_f).

IV.B. ZNMF Based Forcing

The forcing frequencies have been selected based on the shear layer and separation bubble frequencies of the baseline uncontrolled flow. As listed in table 1, based on f^*_{sep} the forcing for three cases (Case 1,2 & 4) are chosen such that $f^*_J = m.f^*_{sep}$, where m=1, 2. In order to investigate whether f^*_J has to be indeed a super-harmonic of f^*_{sep}, a case with m=1.5 (Case 3) has also been selected. For Case 2, the effect of location on forcing is examined by placing the ZNMF jet inside the separation bubble, while for Cases 5 and 6 the frequencies are chosen close to f^*_{SL}.

IV.B.1. Forced flow characteristics

Figure 6 shows the instantaneous spanwise vorticity for all the forced flow cases at the same instant after forcing is initiated. When the flow is subjected to forcing based on the f^*_{sep} ahead of the separation point, the separated vortices tend to remain attached over a greater length of the airfoil figure 6(a,c,d). As f^*_J is increased so does the ability of the shear layer to produce discrete vortices. Also a reduction in size of the discrete vortices is seen, which is not unexpected since an increase in forcing frequency leads to a reduction in the spatial scales of the shear layer. On the other hand, placing the jet within the separation does not seem to have a significant effect on the flow as seen in figure 6(b). Figure 6(e,f) shows forcing near the shear layer frequency leads to the formation of smaller discrete vortices which eventually merge to form a strong clockwise vortex at a much lower frequency than that of the naturally separating shear layer. This indicates the rolling-up coalescence phenomenon under forcing as mentioned by Wu et al.[9]

Mean streamlines seen in figure 7 show the effect of forcing on the separation bubble characteristics. It is seen that for f^*_J=2,3 & 4 and x_J/c =0.024 the length of separation bubble is reduced by nearly 54%, 53% and 61% respectively, while H_{sep} is reduced by nearly 80% for all the three cases. On the other hand when f^*_J=2 & x_J/c =0.070, only 30% reduction is seen in L_{sep}. This suggests that forcing at frequencies near to f^*_{sep} ahead of the unstable shear layer generates a better response in controlling separation than placing the jet inside the separation bubble. It might also be possible that placement inside the separation bubble requires a higher momentum coefficient to generate a similar response. Forcing at f^*_J=8 & 10 increases the recirculation region which now extends over most of the surface of the airfoil due to the presence of larger separating vortices.

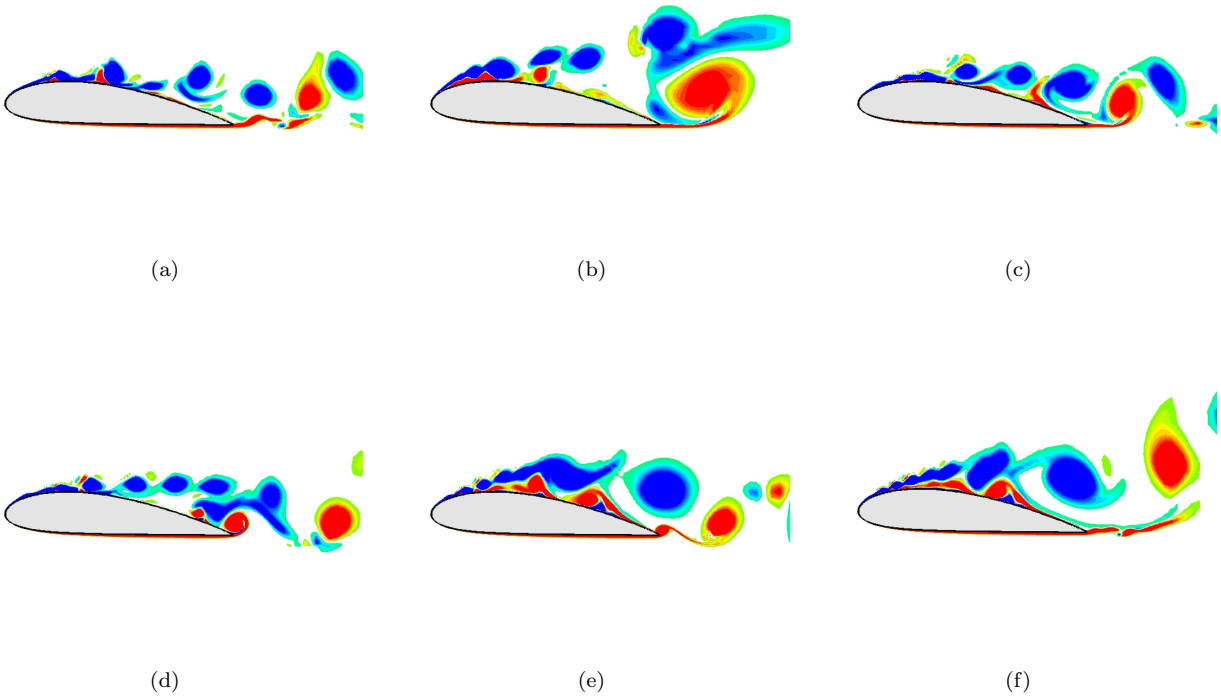

Figure 6. Instantaneous spanwise vorticity corresponding to (a) $f_J^* = 2, x_J/c = 0.024$**,(b)** $f_J^* = 2, x_J/c = 0.070$**, (c)** $f_J^* = 3, x_J/c = 0.024$**,(d)** $f_J^* = 4, x_J/c = 0.024$**, (e)** $f_J^* = 8, x_J/c = 0.024$ **and (f)** $f_J^* = 10, x_J/c = 0.024$**. Contour levels correspond to figure 4(a).**

Control of separation would ideally mean that the flow remains attached over most part of the airfoil and in this particular situation with a leading edge separation, it can be examined based on th trajectory of the separated vortices. Figure 8 shows the comparison of the trajectories of separation bubble vortices for three representative cases to the baseline case. For f_J^*=2 & x_J/c =0.024, discrete vortices are usually found to be smaller and tend to move closer to the airfoil surface, while f_J^*=10 & x_J/c =0.024 performs poorly in this regard where these vortices travel at a greater distance from the airfoil surface. Note that for the latter case the vortices tend to follow a straight path till about x/c=0.3 and after which the vortices follow the path of the baseline case.

Based on our observations, a clearer picture emerges regarding the flow response at the high frequencies that are in the vicinity of the natural shear layer frequency. For the baseline uncontrolled flow, the shear layer evolves in the vicinity of the separation region and its dynamics are substantially modified through interactions in this proximity. In particular, formation of separation bubble vortices allows for mixing of high momentum outer flow into the separated region and tend to mitigate to some extent the effect of the adverse pressure gradient consequently moving the shear layer closer to the airfoil surface which is the case when forcing is based on the natural separation region frequency. In contrast, when the shear layer is forced at or close to its natural frequency it evolves relatively independent of the dynamics of the separation region. Consequently, the shear layer moves in almost a straight line from the point of separation resulting in a larger separation region over the airfoil. Thus, even though the effect of forcing at higher frequency is not the desired one in the current context, the effect is nevertheless interesting since it provides further insights into both the uncontrolled and controlled flow cases.

The averaged pressure coefficient for the three representative control cases are compared with the baseline case in figure 9(a). The suction peaks for the controlled cases are found to be higher than the baseline case. Overall for the control case with f_J^*=2 & x_J/c=0.024, smooth pressure recovery is obtained till the trailing edge, however when the jet location is changed to x_J/c=0.070 the pressure distribution reflects characteristics similar to that of the baseline flow with a smaller separated region. For the case with f_J^*=10 the suction peak is followed by a large plateau, extending from x/c ∼0.18 to the nearly the trailing edge of the airfoil. The

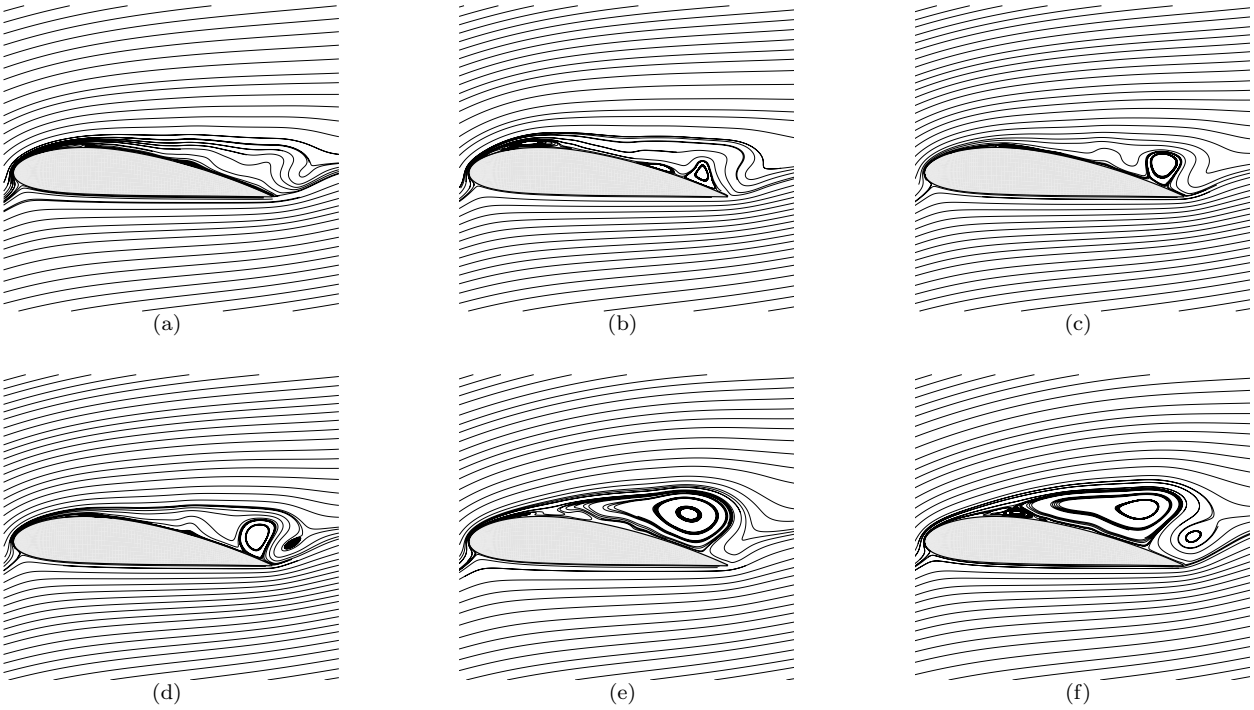

Figure 7. Mean streamlines corresponding to (a) $f_J^* = 2, x_J/c = 0.024$**, (b)** $f_J^* = 2, x_J/c = 0.070$**,(c)** $f_J^* = 3, x_J/c = 0.024$**,(d)** $f_J^* = 4, x_J/c = 0.024$**,(e)** $f_J^* = 8, x_J/c = 0.024$ **and (f)** $f_J^* = 10, x_J/c = 0.024$**.**

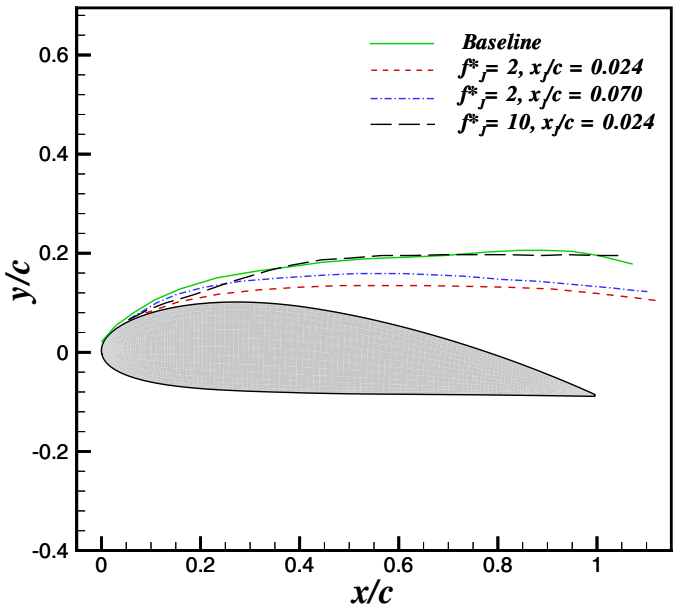

Figure 8. Comparison of the trajectory of separation bubble vortices for representative cases.

trailing edge shows higher pressure on the suction side in comparison to the baseline case. Further insight of separation control can be gained by examining the detailed characteristics of the flow in terms of the skin friction coefficient as seen in figure 9(b). As mentioned earlier forcing ahead of the separation at f_J^*=2 gives the maximum separation control of the three cases. Forcing at this frequency inside the separation bubble reduces the magnitude of separation, however, the skin fiction distribution is similar to the baseline flow. The sharp drop near x/c=0.07 in skin friction corresponds to the location of the ZMNF jet. At higher frequency the separation extends for most part of the airfoil and the skin friction increases sharply around $x/c \sim 0.81$. This is due to the rollup of the trailing edge shear layer onto the top surface corresponding to the increase in pressure in this region, see figure 7(f).

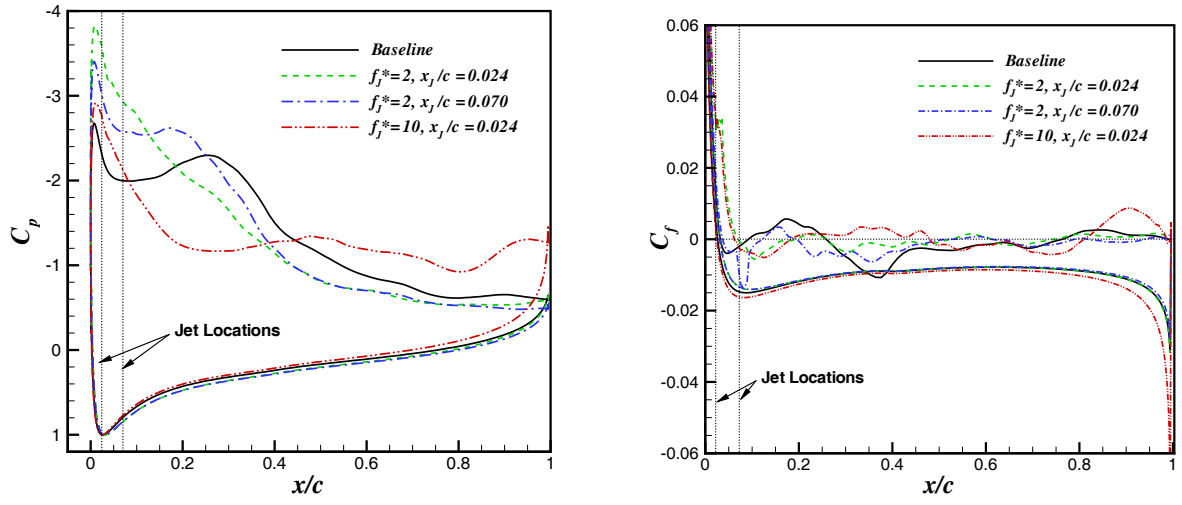

(a) (b)

Figure 9. Comparison of the time-averaged(a) pressure coefficient and (b) skin friction coefficient of baseline and controlled cases (the horizontal dotted line represents zero mean for C_f).

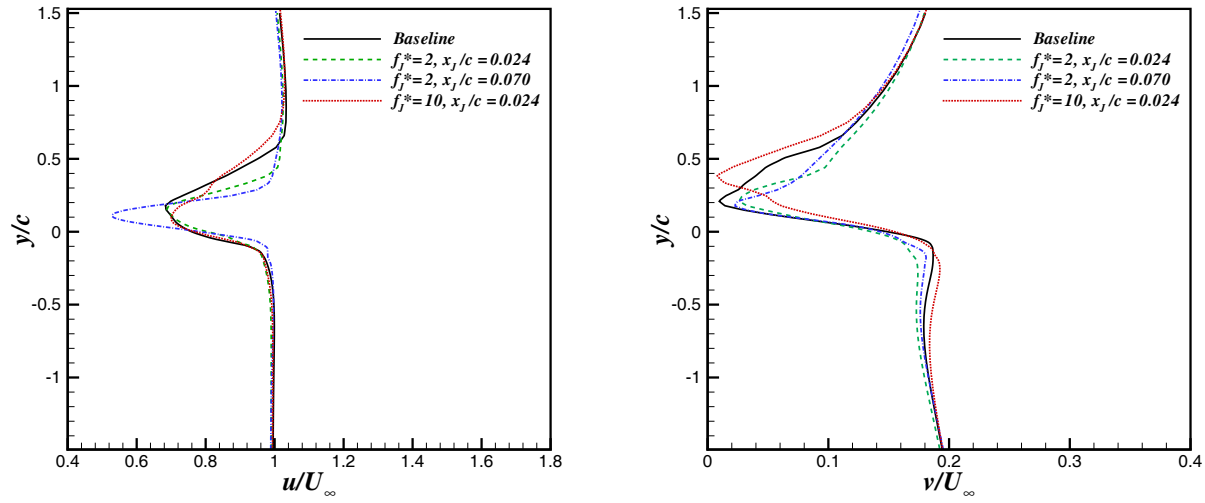

(a) (b)

Figure 10. Comparison of the mean (a) streamwise and (b) crosstream velocity profiles in the wake at x/c=1.5.

The effect of forcing on the airfoil wake is also examined for select cases. As expected for f_J^*=2 & x_J/c=0.024, there is a narrowing of the wake with the same amount of streamwise velocity deficit as the baseline case as seen in figure 10(a), interestingly however moving the jet within the separation bubble leads to higher velocity deficit with a narrower wake. This indicates that although the wake is narrower, increased deficit will lead to a corresponding increase in pressure drag. Glezer et al.[10] have also observed an increase

in deficit with narrowing of wake at low frequencies. For higher forcing frequency there is an asymmetric increase in the width of the wake with a slight reduction in the deficit. Figure 10(b) show the crossstream velocity in the wake which at lower frequencies exhibit similar characteristics with only a marginal difference in deficit and while an upward shift is seen at higher frequency due to the modification of the wake when stronger vortices are formed.

IV.B.2. Effect of Forcing on Temporal Characteristics of Flow

It is known that the shear layer is able to lock-on to the forcing frequency or its super-harmonic, which is necessary for effective shear layer control.[9] In figure 11 we show the frequency spectra for the various forced cases which allows us to examine the effect of forcing frequency on the temporal characteristics of the forced flow. For the first case where $f_J^* = 2$ & $x_J/c = 0.024$, we find that both the shear layer and the separation bubble show a distinct lock-on to the forcing frequency. The wake still exhibits a broad peak extending from about $fc/U_\infty = 1$ to $fc/U_\infty = 2$ which indicates that the wake retains most of its natural dynamics but at the same time shows some effect of the forcing frequency. It should be noted that the narrowing of the wake due to forcing would also tend to increase the natural frequency of the wake.

The next case is at the same forcing frequency, however the forcing location is shifted to $x_J/c = 0.07$ which is downstream of the separation point and inside the separation bubble. For this case, the separation bubble does lock-on to the forcing frequency. However, unlike the previous case, the shear layer does not show a distinct response at the forcing frequency which is inline with the fact that the forcing is located downstream of the separation point. For $f_J^* = 3$ & 4 the response to forcing is similar to that of $f_J^* = 2$ at $x_J/c = 0.024$. Both the shear layer and the separation bubble lock-on to the forcing frequency but the wake seems unaffected and retains a dominant peak at its natural frequency. This suggests that forcing at a frequency which is not a super-harmonic of the separation bubble frequency might also be able to elicit a favorable separation control, however further studies are required to confirm this observation.

The last two cases seen in figure 11(e,f) correspond to high frequency forcing and both show a very similar response which is distinctly different from all the previous cases. First, although the shear layer locks-on to the forcing frequency, both the separation region and the wake exhibit virtually no response to the forcing. This is clearly due to the fact that the high frequency is well outside the receptive range for these regions. Interestingly though, the separation region and the wake show very similar power spectra indicating that these two regions have effectively merged into one and no longer show distinct dynamics. Furthermore, the dominant frequency in this region shifts to a lower frequency of about 0.5 and this is consistent with the formation of large clockwise vortices on the suction surface resulting from the merger of many shear layer vortices. Thus even though the high frequency forcing does not couple directly with the separation bubble or the wake region, its effect on these regions is quite substantial.

In general we observe that varying the forcing frequency has a distinct effect on the natural characteristics of the flow. Forcing near the natural separation bubble frequency ahead of the separation tends to modify both the shear layer and separation bubble characteristics without having a significant effect on the wake. Thus, by locking onto the local instability of the flow it is possible to control the leading edge separation. In addition, this instability is most receptive to forcing ahead of the separation as was also observed in an earlier study.[17] However, when forcing at frequencies close to that of the shear layer although only the shear layer is able lock-on to the forcing, global modification of the flow due to modification of wake and separation bubble characteristics can be attained.

IV.B.3. Aerodynamic Performance

Aerodynamic performance of the airfoil in response to forcing is examined by comparing the averaged total lift and drag coefficients along with the lift-to-drag ratios. Figure 12(a) compares the drag coefficients to the baseline case. It is found that frequencies closer to the f_{sep}^* show significant reduction in the drag with f_J^*=2 & $x_J/c = 0.024$ showing approximately 30% decrease while the higher forcing frequencies increase the drag by nearly 40-50%. This however is not the case for the lift as shown in figure 12(b). For f_J^*=2 and f_J^*=10 lift decreases slightly while for f_J^*=3, 4 & 5 there is a marginal increase in the lift. The percentage difference of individual control cases to the baseline case are listed in table 2.

Comparison of the lift-to-drag ratio in figure 12(c) shows overall improvement in this quantity by nearly 40% for f_J^*=2, $x_J/c = 0.024$ case while for f_J^*= 3 & 4 , the increase is nearly 28-29%. The higher frequency

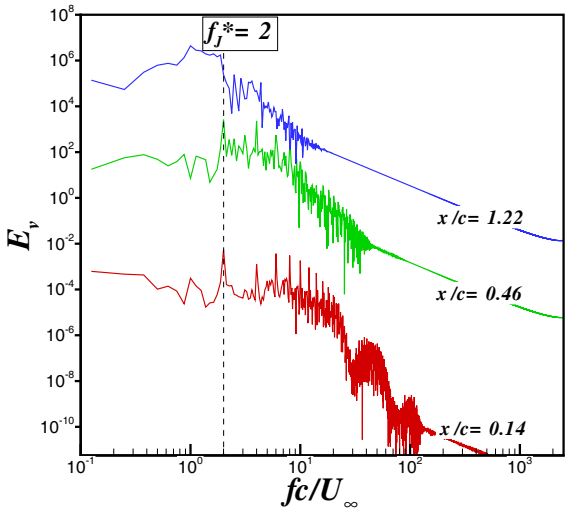

(a) $f_J^* = f_{sep}^*, x_J/c = 0.024$

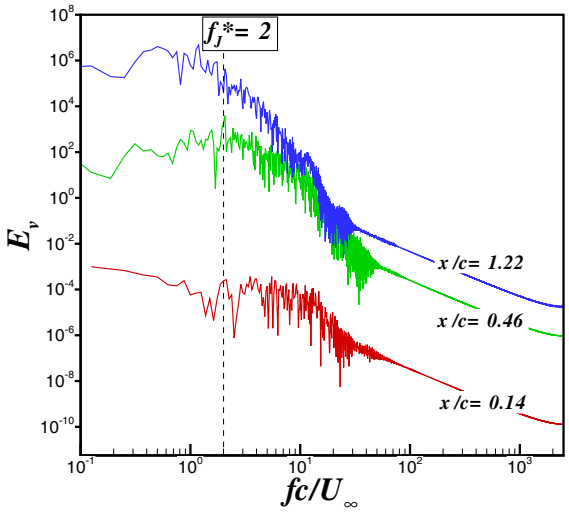

(b) $f_J^* = f_{sep}^*, x_J/c = 0.070$

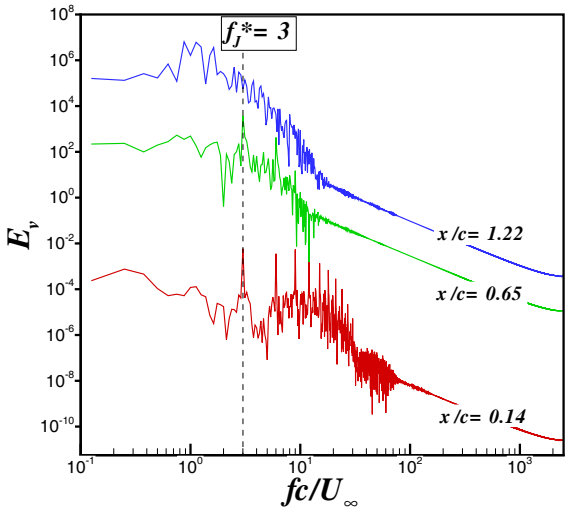

(c) $f_J^* = 1.5 f_{sep}^*$

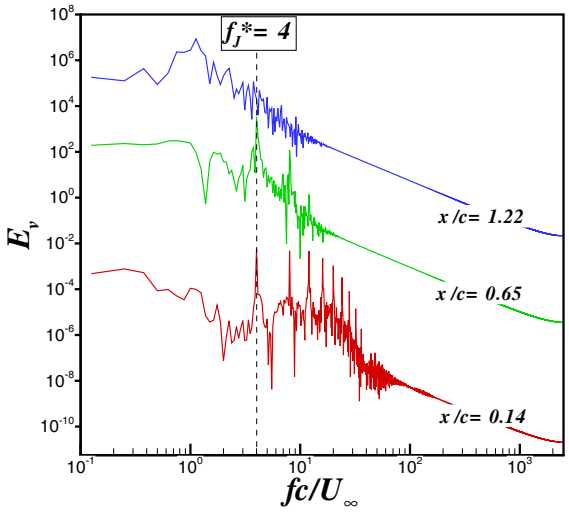

(d) $f_J^* = 2 f_{sep}^*$

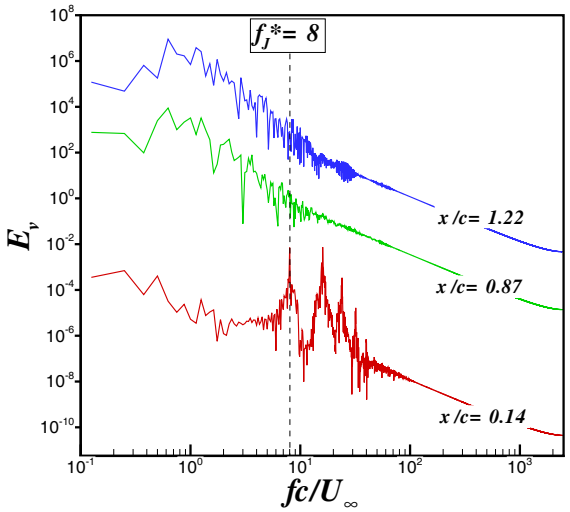

(e) $f_J^* = 0.8 f_{SL}^*$

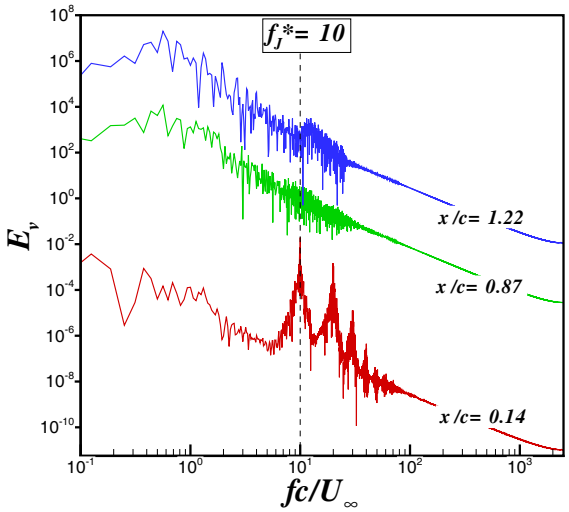

(f) $f_J^* = f_{SL}^*$

Figure 11. Frequency spectra of cross-stream velocity for (a) $f_J^* = 2, x_J/c = 0.024$,(b) $f_J^* = 2, x_J/c = 0.070$, (c) $f_J^* = 3, x_J/c = 0.024$,(d) $f_J^* = 4, x_J/c = 0.024$, (e) $f_J^* = 8, x_J/c = 0.024$ and(f) $f_J^* = 10, x_J/c = 0.024$; the bottom, middle and top lines represent the forced shear layer, separation and wake frequencies respectively. The values have been offset in y-axis for distinction.

cases show a decrease up to 40% in the lift-to-drag ratio. Since forcing inside the separation bubble shows a slight decrease in both drag and lift its lift-to-drag ratio is similar to that of the baseline case.

Table 2. Percentage variation of lift,drag coefficients and lift-to-drag ratio for the controlled cases

$f_J c/U_\infty$	x_J/c	C_d	C_l	C_l/C_d
f^*_{sep}	0.024	-29.68	-1.97	+39.40
f^*_{sep}	0.070	-9.93	-10.53	-0.66
$1.5f^*_{sep}$	0.024	-17.08	+7.05	+29.12
$2.0f^*_{sep}$	0.024	-16.70	+6.72	+28.12
$0.8f^*_{SL}$	0.024	+41.34	+2.22	-27.67
f^*_{SL}	0.024	+50.89	-9.71	-40.16

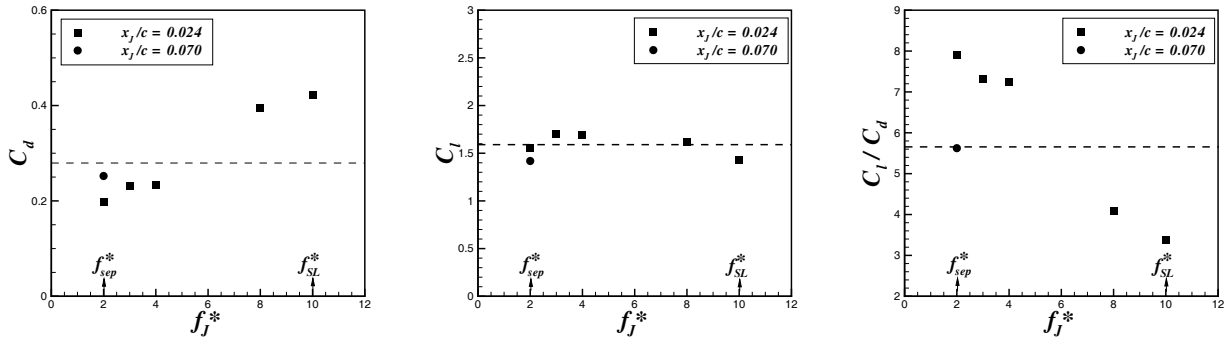

(a) (b) (c)

Figure 12. Comparison of (a) drag coefficient,(b) lift coefficient and (c) lift-and-drag ratio for controlled cases as a function of frequency and location. The dashed line indicates the baseline case value.

V. Conclusion

Detailed analysis of a post-stall flow over an airfoil at Re_c=40,000 has been conducted using 2-D time-accurate simulations. The separated flow displays three distinct natural frequencies corresponding to the shear layer, separation bubble and wake. The shear layer and separation bubble frequencies for the uncontrolled flow are used as the basis for selecting the ZNMF jet forcing frequencies. In addition to providing forcing ahead of the separation bubble, forcing is also provided inside it to observe the effect of location.

Forcing at or near the separation bubble frequency ahead of the separation point provides effective reduction in separation and a significant increase in the lift-to-drag ratio. In particular, by forcing at these frequencies, it is possible to control the local instability in the natural flow which leads to the leading edge separation. When the excitation frequency is closer to the shear layer frequency, the shear layer evolves independent of the dynamics of the flow. This phenomenon results in large vortices which tend to increase the size of the separation bubble and wake while reducing the frequency of vortex shedding. Placing the jet inside the separation bubble does not improve the lift-to-drag ratio. Overall it was found that improvement in the aerodynamic performance was obtained primarily due to reduction in drag while there was no significant effect on the lift coefficient. Work is currently underway to study the effects of forcing based on the wake frequency. In addition 3-D studies at higher angles of attack are also being carried out.

VI. Acknowledgements

This work is supported by U.S. Air Force Office of Scientific Research grants (FA9550-05-0169 to RM and FA9550-05-0093 to LC). The authors are thankful to Dr. Reza Ghias for useful discussions and inputs.

References

[1]Hsiao, F., Liu, C.-F., and Shyu, J.-Y., "Control of Wall-separated flow by Internal Acoustic Excitation," *AIAA Journal*, Vol. 28, No. 8, 1990, pp. 1440–1446.

[2]Seifert, A., Darabi, A., and Wygnanski, I., "Delay of Airfoil Stall by Periodic Excitation," *Journal of Aircraft*, Vol. 33, No. 4, 1996, pp. 691–698.

[3]Zaman, K., Bar-sever, A., and Mangalam, S., "Effect of acoustic excitation on the flow over a low-Re airfoil," *Journal of Fluid Mechanics*, Vol. 182, 1987.

[4]Seifert, A., Eliahu, S., Greenblatt, D., and Wygnanski, I., "Use of piezoelectric actuators for airfoil separation control," *AIAA Journal*, Vol. 36, No. 8, 1998, pp. 1535–37.

[5]Seifert, A. and Pack, L., "Oscillatory Control of Separation at High Reynolds Numbers," *AIAA Journal*, Vol. 37, No. 9, 1999, pp. 1062–1071.

[6]Amitay, M., Smith, D., Kibens, V., Parekh, D., and Glezer, A., "Aerodynamics Flow control over an Unconventional Airfoil USing Synthetic Jet Actuators," *AIAA Journal*, Vol. 39, No. 3, 2001, pp. 361–370.

[7]Amitay, M., Smith, B., and Glezer, A., "Aerodynamic Flow control using Synthetic Jet Techonolgy," AIAA Paper 98-0208, 1998.

[8]Glezer, A. and Amitay, M., "Synthetic Jets," *Annual Review of Fluid Mechanics*, Vol. 34, 2002.

[9]Wu, J., Lu, X., Denny, A., Fan, M., and Wu, J., "Delay of Airfoil Stall by Periodic Excitation," *Journal of Aircraft*, Vol. 371, 1998, pp. 21–58.

[10]Glezer, A., Amitay, M., and Honohan, A., "Aspects of Low- and High-Frequency Actuation for Aerodynamic Flow Control," *AIAA Journal*, Vol. 43, No. 7, 2005, pp. 1501–1511.

[11]Pack, L. G., Schaeffler, N. W., Yao, C.-S., and Seifert, A., "Active Control of Flow Separation from the Slat Shoulder of a Supercritical Airfoil," AIAA Paper 2002-3156, 2002.

[12]Greenblatt, D. and Wygnanski, I., "Effect of Leading-Edge Curvature on Airfoil Separation Control," *Journal of Aircraft*, Vol. 43, No. 3, 2003, pp. 473–481.

[13]Mittal, R., Kotapati, R., and Cattafesta, L., "Numerical Study of Resonant Interactions and Flow Control in a Canonical Seperated Flow," AIAA Paper 2005-1261, 2005.

[14]Roshko, A., "On the Development of Turbulent Wakes from Vortex Sheets," NACA Report No. 1191, 1954.

[15]Ho, C. M. and Huerre, P., "Perturbed free shear layers," *Annual Review of Fluid Mechanics*, Vol. 16, 1984.

[16]Mittal, R. and Kotapati, R., "Resonant Mode Interaction in a Canonical Separated Flow," *Proceedings of the Sixth IUTAM Symposium on Laminar-Turbulent Transitions*, Springer, Banglore, India, 2004.

[17]Kotapati, R., Mittal, R., and Cattafesta, L., "Numerical Experiments in Synthetic Jet Based Separation Control," AIAA Paper 2006-0320, 2006.

[18]Zaman, K. and Culley, D., "A study of Stall control over an Airfoil using 'Synthetic Jets'," AIAA Paper 2006-98, 2006.

[19]Ghias, R., Mittal, R., and Lund, T., "A Non-Body Conformal Grid Method for Simulation of Compressible Flows with Complex Immersed Boundaries," AIAA Paper 2004-80, 2004.

[20]Ghias, R., Mittal, R., and Dong, H., "A Sharp Interface Immersed Boundary Method for Compressible Viscous Flows," *Journal of Computational Physics (accepted)*.

[21]Anderson, A., Tannehill, C., and Pletcher, R., *Computational Fluid Mechanics and Heat Transfer*, Hemisphere Publishing Corporation, New York, 1984.

[22]Leonard, B. P., "A stable and accurate on convection modeling procedure based on quadratic upstream interpolation," *Computer Methods in Applied Mechanics and Engineering*, Vol. 19, 1979, pp. 59–98.

[23]Kennedy, C., Carpenter, M., and Lewis, R., "Low-storage, explicit Runge-Kutta scheme for the compressible Navier-Stokes equations," ICASE Report No. 99-22, 1999.

[24]Mittal, R. and Balachandar, S., "Effect of Three-Dimensionality on the Lift and Drag of Nominally Two-Dimensional Cylinders," *Physics of Fluids*, Vol. 7, No. 8, 1995, pp. 1841.